Microchimica Acta (2023) 190:317
https://doi.org/10.1007/s00604-023-05896-8

ORIGINAL PAPER

Mn-MOF catalyzed multi-site atom transfer radical polymerization electrochemical sensing of miRNA-21

Jiao Wang[1] · Jingliang Liu[2] · Lianzhi Li[3] · Jinming Kong[1] · Xueji Zhang[4]

Received: 7 March 2023 / Accepted: 1 July 2023 / Published online: 24 July 2023

Abstract

A green electrochemical biosensor was developed based on metal-organic framework (MOF)-catalyzed atom transfer radical polymerization (ATRP) for quantifying miRNA-21, used as the proof-of-concept analyte. Unlike conventional ATRP, Mn-PCN-222 (PCN, porous coordination network) could be used as an alternative for green catalyst to substitute traditional catalysts. First, poly (diallyldimethylammonium chloride) (PDDA) was fixed on the surface of the indium tin oxide (ITO) electrode, and then the Mn-PCN-222 was linked to ITO electrode via electrostatic binding with PDDA. Next, aminated ssDNA (NH_2-DNA) was used to modify the electrode further by amide reaction with Mn-PCN-222. Then, the recognition and hybridization of NH_2-DNA with miRNA-21 prompt the generation of DNA−RNA complexes, which further hybridize with Fc-DNA@β-CD-Br_{15} and permit the initiator to be immobilized on the electrode surface. Accordingly, β-CD-Br_{15} could initiate the polymerization of ferrocenylmethyl methacrylates (FcMMA) under the catalysis of MOF to complete the ATRP reaction. FcMMA presented a distinct electrochemical signal at ~ 0.33 V. Taking advantage of the unique multi-site properties of β-CD-Br_{15} and the efficient catalytic reaction induced by Mn-PCN-222, ultrasensitive detection of miRNA-21 was achieved with a detection limit of 0.4 fM. The proposed electrochemical biosensor has been applied to the detection of miRNA-21 in serum samples. Therefore, the proposed strategy exhibited potential in early clinical biomedicine.

Keywords MOF · ATRP · β-CD-Br_{15} · Host-guest interaction · miRNA-21 · Square-wave voltammetry

Introduction

Lung cancer is the primary cause of cancer deaths in the world, accounting for more deaths than breast, colorectal, and prostate cancers combined [1, 2]. Early detection of lung cancer provides more opportunities prevention and treatment, thus improving patient prognosis [3]. Currently, detecting serum biomarker levels is the best way for lung cancer screening with a sensitivity of ca. 80% [4, 5]. However, the poor specificity of biomarker testing often leads to needless lung biopsy and excessive therapy, particularly in diagnostic gray area [6, 7]. Fortunately, microRNAs are prospective biomarkers for the diagnosis of lung cancer [8–10]. miRNA-21 is upregulated in many types of human tumors and adjacent tissues, while serum miRNA-21 overexpression has been demonstrated in different cancers, such as lung cancer, prostate cancer, or breast cancer [11–14]. Therefore, miRNA-21 can be used as a marker for many human tumors, and microdetection of miRNA-21 can help in the early diagnosis of tumors. Lung cancer–derived miRNA-21 testing is a promising alternative to standard biopsies, enabling minimally invasive, precise, and early treatment of lung cancer. Existing methods for miRNA detection include electrochemistry [13], RNA blotting [13], quantitative polymerase chain reaction [11], etc. Nanotechnology employing polymers [15], inorganic particles [16], liposomes [17], carbon materials [18], metallic materials [19], and their composites has

Jiao Wang and Jingliang Liu contributed equally.

✉ Jinming Kong
j.kong@njust.edu.cn

1 School of Environmental and Biological Engineering, Nanjing University of Science and Technology, Nanjing, Jiangsu 210094, People's Republic of China

2 School of Environmental Science, Nanjing XiaoZhuang University, Nanjing 211171, People's Republic of China

3 School of Chemistry and Chemical Engineering, Liaocheng University, Liaocheng 252059, People's Republic of China

4 School of Biomedical Engineering, Shenzhen University Health Science Center, Shenzhen, Guangdong 518060, People's Republic of China

emerged as prospective platforms for diagnosis and treatment of lung cancer over the past few decades, contributing to lower mortality and longer lifetime. The well-designed nanomaterial for lung cancer treatment is expected to conquer a series of biological obstacles and traps, and improve the treatment outcomes with fewer side effects.

Metal-organic frameworks are composed of organic linkers and inorganic metal nodes (or clusters), which are of interest for their high specific surface area, porous structure, good stability and diverse functionalities [20, 21]. These characteristics contribute to an increasing trend of analyte aggregation and facilitate fast mass transfer of analytes over large surface areas, making MOFs bring desired functions for electrochemical treatment of cancer [22, 23]. Therefore, MOFs can not only provide an alternative to now available nanomaterials for cancer therapy but also have great potential in filling the dependence of nanomedicine on biological ligands (e.g., immunogenicity, stability, applicability, and cost). MOFs generally have six series such as Isoreticular Metal-Organic Framework (IRMOF) [24], Zeolitic imidazolate framework (ZIF) [25], Coordination Pil1ared-Layer (CPL) [26], Materials of Institut Lavoisier (MIL) [27], Porous Coordination Network (PCN) [28], University of Oslo (UIO) [29]. Among them, the PCN series with porphyrin and metalloporphyrin as ligands are particularly prominent. On account of metalloporphyrins's p-conjugated macrocyclic structures, Mt-PCN exhibits excellent electron transfer and selective redox catalytic performance [30, 31], befitting for electrochemical detection of a variety of target analytes [32, 33]. Therefore, in this method, a prototypical PP-MOF (Mn-PCN-222) constructed from Zr_6 cluster and Mn(III) meso-tetrakis(4-carboxyphenyl)-porphyrin chloride (MnTBAP) ligand was employed. The prepared Mn-PCN-222 possessed numerous virtues as a biomimetic catalyst. We also compared the properties of Mn-PCN-222 with previously reported literature. As could be seen from Table S2, Mn-PCN-222 had many characteristics, such as simulated enzyme activity, photocatalytic properties, intracellular fluorescence imaging, etc. This is enough to show that the Mn-PCN-222 has a variety of application fields, and at the same time can solve some important problems in the field of scientific research. This can be attributed to the following three points: firstly, Mn(III) ion was coordinated with the N atom on the porphyrin ring to form MnTBAP, and in most cases Mn is difficult to separate from the porphyrin ring; thus, it will improve the catalytic lifetime of Mn-PCN-222 and eliminate product contamination [34]. Second, its particular metal coordination could avoid numerous side reactions in the catalytic procedure, improving the catalytic efficiency [34]. Third, Mn-PCN-222 is a green catalyst and will not introduce heavy metal ions into the system.

ATRP is gaining attention as a reliable signal amplification method in the detection of clinically important biomolecules, such as nucleic acids and proteins [35, 36]. For example, exonuclease-mediated atom transfer radical strategy for nucleic acid detection has been realized in 2021 [37]. A peptide nucleic acid (PNA)-based DNA fragment sensor was proposed using electrochemically controlled ATRP as signal amplification strategy [38]. ATRP was a significant reversible deactivating radical polymerization (RDRP) using alkyl halides (R−X, X = Cl, Br) as initiators, Cu^I/ligand complexes as activators, and corresponding $Cu^{II}X$/ligand complexes as deactivators [39, 40]. The diversity of ATRP initiators, ligands (such as tris[2-(dimethylamino) ethyl] amine (Me_6TREN)) [41], and vinyl monomers (such as (meth)acrylamide and (meth)acrylamide base) acrylate) made ATRP a universal strategy for signal amplification [42]. Nevertheless, the preparation of most monomers and ligands is time consuming, cumbersome, and high cost. Hence, to overcome these shortcomings and improve the monomer polymerization efficiency, a multi-site initiator β-CD-Br_{15} was prepared [43]. Thus, combining the multi-site priming feature of β-CD-Br_{15} and the high catalytic efficiency of Mn-PCN-222, a multi-site initiation-enhanced Mn-PCN-222-based ATRP electrochemical biosensor for analysis of miRNA-21 was proposed. The Mn-PCN-222 reacted with NH_2-DNA through amide reaction, and further ATRP was achieved based on the miRNA-21-initiated specific recognition and host-guest reaction. Compared with traditional ATRP, this method has following advantages: (a) Mn-PCN-222 was a green catalyst with good biocompatibility, no pollution to the environment, it will not introduce additional heavy metal ions into the system; (b) β-CD-Br_{15} possessed 15 initiation sites that can improve the polymerization efficiency of monomers.

Experimental section

Synthesis of Mn-PCN-222

The Mn-PCN-222 nanoparticles were prepared employing a solvo-thermal method. $ZrOCl_2 \cdot 8H_2O$ (26 mg), Mn (III) meso-tetra (4-carboxyphenyl) porphine chloride (MnTBAP) (12 mg), and benzoic acid (225 mg) were dissolved in 2 mL DMF and then the mixture was sonicated for 10 min. The reaction precursor was then heated at 80°C for 24.0 h. After the above solution was slowly cooled to room temperature, the collected Mn-PCN-222 was rinsed with fresh N, N-dimethylformamide (DMF) and ethanol via centrifugation (10,000 rpm) for three times. Finally, the Mn-PCN-222 was dried under vacuum at 50°C for 12.0 h.

Fabrication of NH_2-DNA/MOF/P/ITO

First, the newly washed ITO electrode was soaked into 1% poly(diallyl dimethylammonium chloride) (PDDA) solution for 1.0 h at 37°C to form a positively charged electrode (P/ITO). Then 15 µL of 1 mg/mL Mn-PCN-222 was coated onto the P/ITO electrode surface and dried at room temperature to acquire the MOF/P/ITO electrode. Subsequently, the MOF/P/ITO electrode was soaked in 1 mM ascorbic acid (AA) solution. Finally, the obtained MOF/P/ITO was incubated with 20 µL of 1 µM NH_2-DNA for 2.0 h to fabricate NH_2-DNA/Mn/P/ITO electrode.

Host-guest interaction

The host-guest interaction between β-CD-Br_{15} (1 mg/mL) and Fc-DNA (1 µM) was achieved in PBS at 37°C for 2.0 h.

Electrochemical analysis of miRNA-21

For electrochemical biosensing, the NH_2-DNA/MOF/P/ITO was coated with 20 µL of different concentrations of miRNA-21 for 2.0 h to form miRNA/NH_2-DNA/ MOF/P/ITO electrode. Following that, the resulting electrode was incubated with 15 µL of β-CD-Br_{15}@Fc-DNA for 2.0 h. After the electrode was rinsed with water, it was immersed in 500 µL of FcMMA (4 mM) solution at 48°C to trigger ATRP. Finally, the SWV signals of the sensing system were determined with the potential from 0 to 0.7 V, a scanning frequency of 15 Hz, an amplitude of 0.025 V, and a step potential of 0.004 V.

Detection of miRNA-21 in human serum samples

To evaluate the practicability of this electrochemical method in human serum samples, standard addition method was used to analyze human serum samples. A 100 µL human serum sample was diluted 10-fold with PB (PH = 7.4) and no further treatment. And the prepared samples were detected according to the aforementioned steps.

Results and discussion

Characterization of Mn-PCN-222

The synthetic route of Mn-PCN-222 is shown in Fig. 1A. Its one-dimensional hexagonal mesopores filled with porphyrin sites make it an efficient sensing lead. In order to verify whether the ideal MOF was synthesized, X-ray diffraction

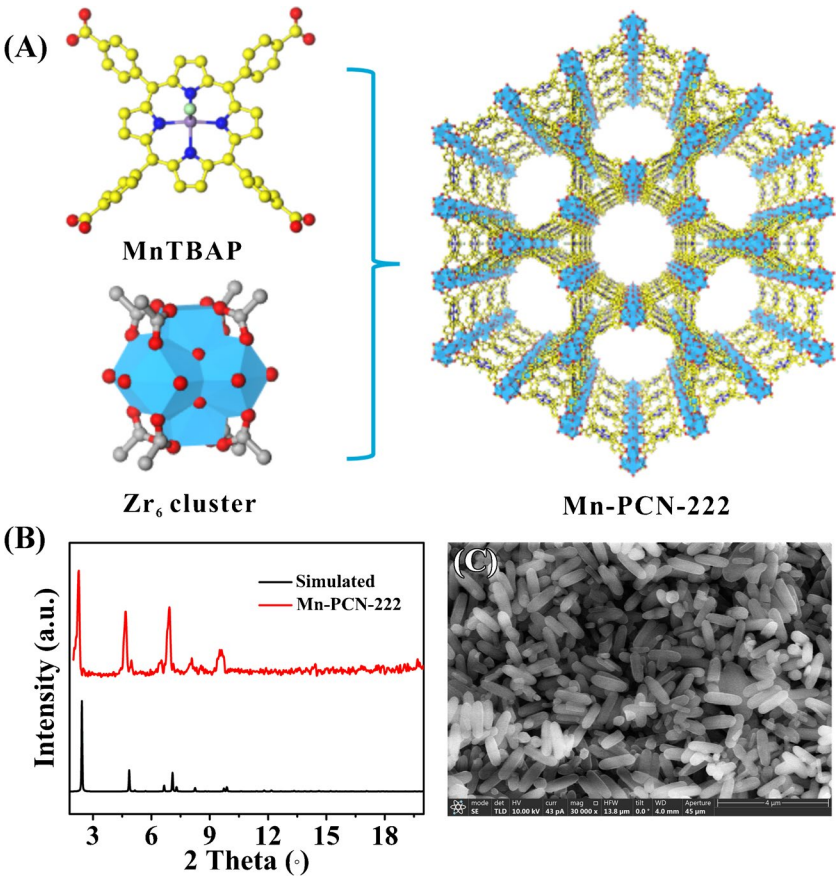

Fig. 1 **A** Diagram of the synthetic route of Mn-PCN-222. **B** Simulated and synthetic XRD spectra of Mn-PCN-222. **C** SEM images of Mn-PCN-222

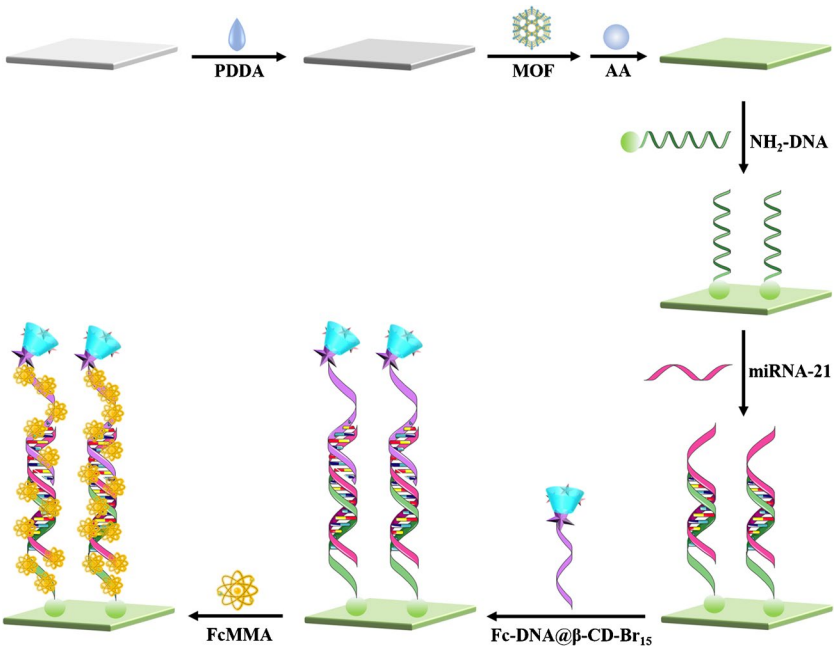

Scheme 1 The schematic diagram of the proposed electrochemical biosensor

(XRD) pattern of Mn-PCN-222 powder was tested (Fig. 1B). These diffraction patterns were consistent with the simulated XRD curves, indicating that the bulk phase purity of crystalline Mn-PCN-222 was relatively high. Further, the morphological feature of Mn-PCN-222 was characterized via scanning electron microscopy (SEM). As described in Fig. 1C, uniform rod-shaped Mn-PCN-222 crystallites with the size of 350 nm × 1 μm were observed. In principle, such Mn-PCN-222 crystallites evenly covered on the surface of electrode could inevitably fabricate a valid electrochemical biosensor. The successful synthesis and valence state of Mn-PCN-222 were verified by X-ray photoelectron spectroscopy (XPS). Some peaks were observed at 180 eV, 284 eV, 398 eV, 530 eV, and 642 eV corresponding to Zr 3d, C 1S, N 1s, O 1S, and Mn 2p (Fig. S1A), which was assigned to Fig. S1B–1F. The transmission electron microscopy (TEM) image of Mn-PCN-222 is presented in Fig. S2A. It is clear that Mn-PCN-222 nanoparticles have a rod-like structure with particle size ranging from 1 to 2 μm. The elemental composition of the synthesized Mn-PCN-222 was confirmed by energy dispersive spectroscopy (EDS) analysis (Fig. S2B). The results manifested that Zr, C, N, O and Mn were evenly distributed in the particles, and Mn accounts for a relatively large proportion, which further indicated that Mn was embedded in Mn-PCN-222. TGA analysis of Mn-PCN-222 is described in Fig. S2C, exhibiting a first step loses about 40% weight at 180°C, which may correspond to a loss of moisture content. Then the weight loss of Mn-PCN-222 was almost steady in up to 520°C. It is clear that Mn-PCN-222 have high thermal stability, which reflected the small weight loss of Mn-PCN-222. The Brunauer-Emmett-Taylor (BET) adsorption isotherm models and pore size distribution curve for Mn-PCN-222 are described in Fig. S3A and S3B, respectively. The N_2 isotherm of Mn-PCN-222 was type I, S_{BET} was 1207.7 m^2/g, and the pore size (d) was 2.3 nm, respectively. These results further demonstrate that Mn-PCN-222 has a large surface area and microporous structure, which could be used for electrochemical sensing and improve sensing sensitivity.

Working principle of the Mn-PCN-222-based electrochemical sensor

As shown in Scheme 1, the bare ITO electrode was immersed in PDDA aqueous solutions, so that the electrode surface covered a large number of positive charges. Then, the as-synthesized Mn-PCN-222 nanoparticles were immobilized on the surface of PDDA/ITO by electrostatic adsorption. Subsequently, aminated ssDNA (NH_2-DNA) was linked onto Mn-PCN-222 via amide reaction. After this procedure, once miRNA-21 was introduced, it could partially hybridize with NH_2-DNA to form DNA-RNA complex. Then the unhybridized part in miRNA-21 will hybridize with Fc-DNA@β-CD-Br_{15} to produce NH_2-DNA@miRNA-21@Fc-DNA@β-CD-Br_{15} complex; thus, β-CD-Br_{15} was also usefully connected to the electrode surface. Then, β-CD-Br_{15} triggered ATRP and abundant monomeric ferrocenylmethyl methacrylate (FcMMA) was polymerized on the electrode surface to form $FcMMA_n$/Fc-DNA@β-CD-Br_{15}/miRNA/NH_2-DNA/MOF/P/ITO; thus, a significantly increased square wave voltammetry (SWV) current was visualized. As can be seen from the process of Scheme 2, first, the high-valent metal bromide Mt^{n+1}-Br (Mn^{3+}-Br) forms the low-valent

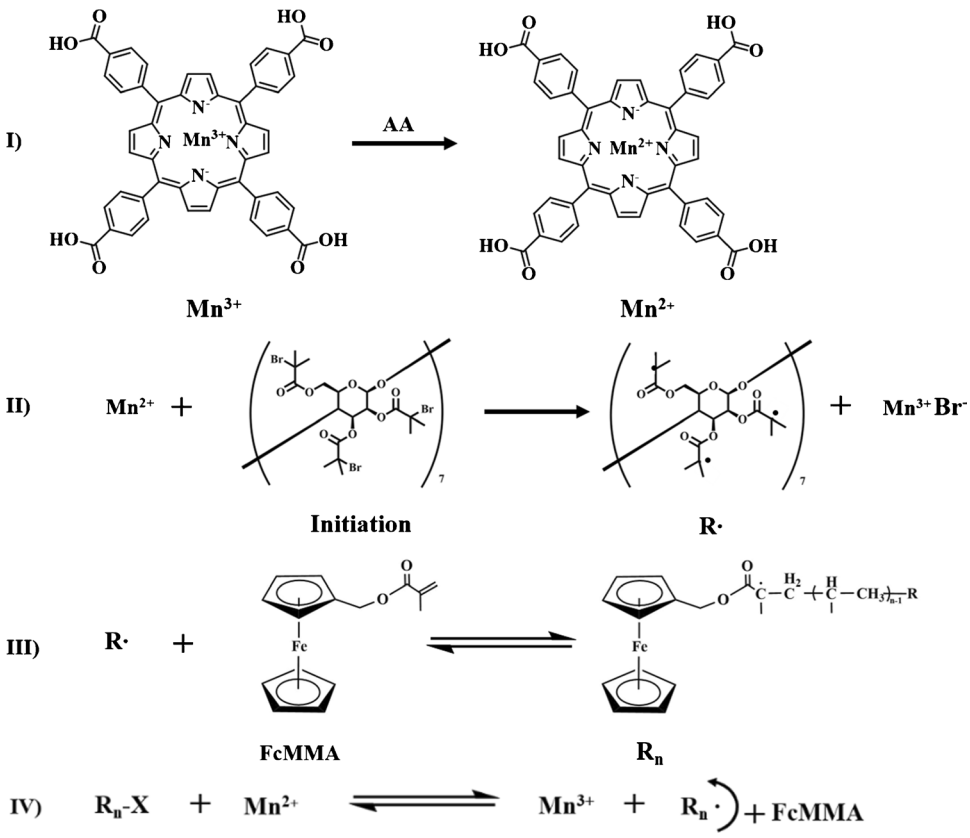

Scheme 2 Mechanism of the proposed ATRP reaction catalyzed via Mn-PCN-222

transition metal complex Mt^n (Mn^{2+}) through the reduction of ascorbic acid (AA). Then in the chain initiation stage, the transition metal complex Mn^{2+} with low valence will firstly obtain Br atom from the organic bromide R-X (initiator β-CD-Br_{15}), and then can generate the high-valence metal bromide Mt^{3+}-Br and the free radical R●, and the AA will become dehydroascorbic acid (DHA). In the next stage of chain growth, the free radical R●-initiated monomer (FcMMA) polymerization can form the chain radical R-FcMMA_n●. After that, the chain radical R-FcMMA_n● can obtain Br atoms from the previous high-valence metal halide Mn^{3+}-Br, and at the same time, the R-FcMMA_n-Br dormant species are formed by the passivation reaction, which will convert the high-valence metal halide Mn^{3+} is reduced to the low-valent complex Mn^{2+}. R-FcMMA_n-Br becomes a new initiator, which can repeat the above-mentioned ATRP reaction, making the chain continue to grow. Therefore, in essence, ATRP could be regarded as a reversible catalytic process. The controllability of the reaction depends on the balance between the generation of free radicals in the activation process and the generation of brominated hydrocarbons in the deactivation process. That is to say, the reversible conversion between the transition metal catalysts Mn^{2+} and Mn^{3+}-Br keeps the amounts of free radicals at a low level.

Characterization of electrode modification

To confirm the preparation of the biosensor, electrochemical impedance spectroscopy (EIS) was characterized to verify for different stages of modified ITO. As depicted in Fig. 2A, charge transfer resistance (R_{ct}) and Warburg impedance (Z_w) in parallel with electrolyte solution resistance (R_s) in series can be equated to EIS. Figure 2A shows the Nyquist curve of the step-by-step modification procedure of the electrode. The R_{ct} corresponding to the high-frequency semicircular arc diameter reflected the charge transfer kinetics of $[Fe(CN)_6]^{3-/4-}$. The bare ITO electrode showed an extremely small semicircular arc (R_{ct} = 157.25 Ω), which indicated the charge transferred rapidly on the surface of ITO electrode. Nevertheless, when PDDA (R_{ct} = 195.30 Ω) and Mn-PCN-222 (R_{ct} = 294.14 Ω,) were gradually anchored to ITO surface, the self-assembled insulating monolayer impeded charge transmission due to steric hindrance. Next, when NH_2-DNA and miRNA-21 were linked to the ITO electrode surface, it could be seen that the semicircular arc increased (R_{ct} = 525.11 Ω, curve d, R_{ct} = 549.42 Ω, curve e) was caused by the repulsion of the negatively charged $[Fe(CN)_6]^{3-/4-}$ from the DNA. Subsequently, when the initiator Fc-DNA@β-CD-Br_{15} hybridized with miRNA-21, the spatial site resistance of the electrode surface varied

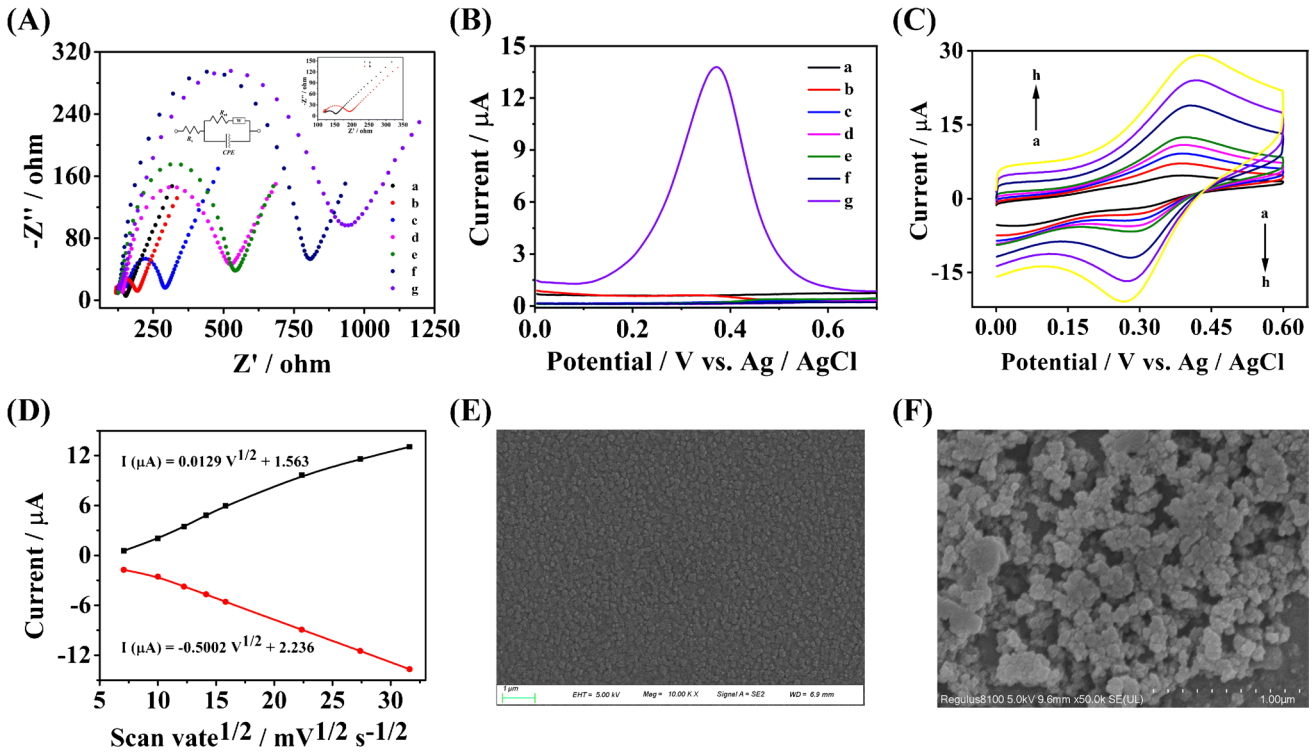

Fig. 2 The EIS (open circuit potential was 0.18 V, the frequency range was 100 kHz to 0.1 Hz, the perturbation potential was 5.0 mV) profile (**A**) and SWV curves (**B**) of the ITO electrodes in different steps: (a) ITO, (b) P/ITO, (c) MOF/P/ITO, (d) NH_2-DNA/MOF/P/ITO, (e) miRNA/NH_2-DNA/MOF/P/ITO, (f) Fc-DNA@β-CD-Br_{15}/miRNA/NH_2-DNA/MOF/P/ITO, and (g) $FcMMA_n$/Fc-DNA@β-CD-Br_{15}/miRNA/NH_2-DNA/MOF/P/ITO. Insert: the equivalent circuit. **C** CV of polymerized FcMMA modified electrode, with scan speeds of 50, 100, 150, 200, 250, 500, 750, and 1000 mV s^{-1}, respectively. **D** Linear relationship between anode (red line) and cathode (black line) currents and the square root of the scanning speed. The SEM images of the ITO electrodes in different steps: **E** bare ITO and **F** $FcMMA_n$/Fc-DNA@β-CD-Br_{15}/miRNA/NH_2-DNA/MOF/P/ITO

and hydrophilicity decreased, resulting in the difficulty of $[Fe(CN)_6]^{3-/4-}$ transfer on the electrode surface and a continuous increase in R_{ct} (= 808.14 Ω). In the end, when a mass of FcMMA monomers were polymerized by ATRP, the electron transfer on ITO surface was impeded, and a R_{ct} of 945.03 Ω was observed. This further confirmed the successful establishment of the proposed electrochemical sensor. Also, the corresponding SWV currents at each modification step were tested to confirm the successful construction of the biosensor (Fig. 2B). In this process, the bare ITO (curve a), P/ITO (curve b), MOF/P/ITO (curve c), NH_2-DNA/MOF/P/ITO (curve d), miRNA/NH_2-DNA/MOF/P/ITO (curve e), and Fc-DNA@β-CD-Br_{15}/miRNA/NH_2-DNA/MOF/P/ITO (curve f) all showed no SWV current. However, an apparent oxidation peak was acquired around ~ 0.33 V (curve g), suggesting FcMMA was polymerized on the electrode surface via ATRP catalyzed by Mn-PCN-222. Furthermore, to confirm that the obtained polymers were modified on the electrode surface by covalent binding instead of non-specific adsorption, electrochemical characterization of $FcMMA_n$/Fc-DNA@β-CD-Br_{15}/miRNA/NH_2-DNA/MOF/P/ITO-modified electrode was performed by cyclic voltammetry (CV) at different scan rates. As described in Fig. 2C, the redox peak current value increased with increasing scan rate. Meanwhile, there is a good linear correlation between the peak current of the anode (red line) and cathode (black line) and the square root of the sweeping speed (50−1000 mV s^{-1}) (Fig. 2D). This proved that the FcMMA was covalently attached to the electrode surface. Further, the bare ITO and the polymerized FcMMA-modified ITO electrodes were also characterized via SEM. As depicted in Fig. 2D, only uniform nanoparticles with the diameter of 25 nm could be seen. The polymerized FcMMA-modified electrode could be seen numerous with nano-flower particles, suggesting that a mass of polymer was produced on the electrode surface.

Feasibility of the Mn-PCN-222-based electrochemical biosensor for miRNA-21 assay

As shown in Fig. 3A, the host-guest interaction between β-CD-Br_{15} and Fc-DNA was achieved in PBS at 37°C. Cyclodextrin is a cyclic oligosaccharide with a molecularly compatible cavity [44]. The cavity can encapsulate organic hydrophobic molecules to form host-guest complexes [45].

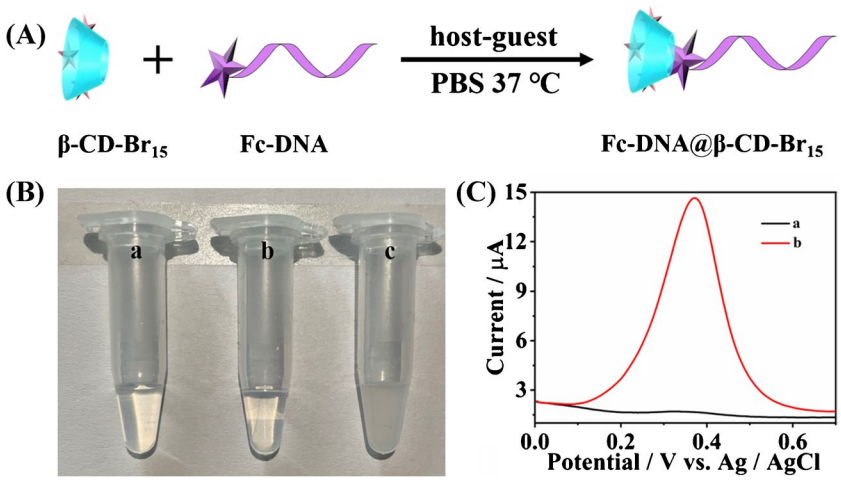

Fig. 3 **A** The host-guest chemistry diagram between β-CD-Br_{15} and Fc-DNA. **B** The photograph: (a) Fc-DNA, (b) β-CD-Br_{15}, and (c) Fc-DNA@β-CD-Br_{15}. **C** The SWV responses of the Mn-PCN-222-based electrochemical biosensor with or without miRNA-21

Ai et al. used cyclodextrin and ferrocene complex for the detection of subgroup J of avian leukosis virus (ALVs-J) [45]. As shown in Fig. 3B, the solution both Fc-DNA and β-CD-Br_{15} was clear; however, the Fc-DNA@β-CD-Br_{15} complex was turbid. This illustrated the successful occurrence of the host-guest interaction Fc-DNA and β-CD-Br_{15}. To further demonstrate the successful construction of the proposed biosensor (Fig. 3C), without miRNA-21 in reaction system, a low SWV current of ca. 0.1390 μA was acquired due to the physical adsorption. When miRNA-21 was present in the system, an obvious SWV current with the value of 12.58 μA could be observed. The calculated signal-to-noise ratio was 90.50, which was contributed to improving sensitivity of the biosensor. Thus, these host-guest and electrochemical results successfully demonstrated that our established MOF-based biosensor was technically feasible to realize analysis of miRNA-21.

Optimization of the experimental conditions

To boost the sensitivity of the electrochemical biosensor, the concentration of β-CD-Br_{15} and the polymerization time of ATRP were optimized. As can be seen from Fig. S4A, the SWV current reached the highest as the amount of β-CD-Br_{15} attained 1.0 mg/mL. However, the SWV signal gradually decreased with β-CD-Br_{15} concentration increasing from 1.5 to 2.0 mg/mL, which may be attributed to the high concentration of initiator that lead to the occurrence of chain termination reaction. Moreover, to facilitate the experimental procedure, the ATRP reaction time was also optimized. As described in Fig. S4B, SWV value reached the maximum when reaction time was around 2.5 h, and the polymerization efficiency of monomers decreases with the extension of ATRP reaction time. One of the reasons for this was that it probably related to the intensification of free radical termination reaction; another reason may be due to the large number of proliferating free radicals embedded in the growing polymer chains, preventing monomer from continuing with the ATRP reaction. Thus, the polymerization time of 2.5 h was used for subsequent experiments, taking into account the concentration of electroactive material enriched and the detection time. As shown in Fig. S4C, the electrochemical response increased as AA concentration ranged from 0.2 to 1.0 mM, but the electrochemical current no longer increased when AA concentration was larger than 1.0 mM, so 1.0 mM was chosen as the optimal experimental concentration for AA. As depicted in Fig. S4D, SWV intensity reached a maximum when FcMMA was 4.0 mM and leveled off when the concentration FcMMA prolonged to 5.0 mM, so 4.0 mM was selected as the optimal concentration.

Quantitative analysis of miRNA-21

To quantitatively evaluate the ability of the Mn-PCN-222-based biosensor to detect miRNA-21, a calibration curve was plotted with the SWV current (I) as ordinate and the miRNA-21 concentration as abscissa. The current rose with the amount of miRNA-21 (Fig. 4A). There was a good relationship between logarithm of different amounts of miRNA-21 and SWV current (Fig. 4B). The linear regression equation was I (μA)= 2.277lg[miRNA-21] + 14.81 (R^2 = 0.9955), and the limit of detection (LOD) was calculated to be 0.4 fM (LOD = $3\sigma/k$, where σ is the standard deviation of the blank and k is the slope of the calibration plot). The electrochemical sensitivity was determined to be 0.0050 μA μM^{-1} cm^{-2}. Moreover, the LOD of this Mn-PCN-222-based miRNA biosensor was lower than that of many other strategies (Table S1). The high sensitivity of this biosensor may be attributed to following factors: (a) multiple initiation sites of β-CD-Br_{15}, promoting the polymerization efficiency of monomers; (b) high catalytic efficiency of Mn-PCN-222; (c) miRNA-21-triggered ATRP signal amplification method. This method had some advantages, and next, we will further reduce the polymerization time to shorten the experimental cycle.

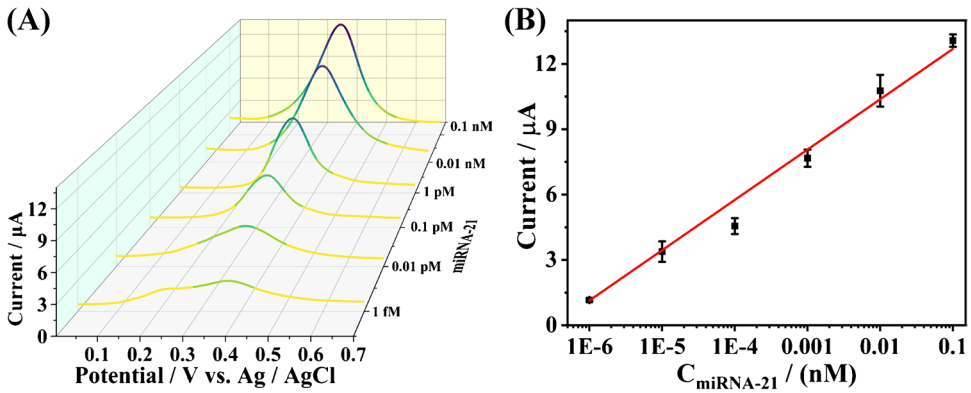

Fig. 4 **A** The SWV currents of Mn-PCN-222-based electrochemical biosensor to different amounts of miRNA-21. **B** Calibration plots between the SWV current value and logarithm of miRNA-21 amount (scanning frequency of 15 Hz, an amplitude of 0.025 V, and a step potential of 0.004 V). Error bars represent the standard deviations of three repeated measurements

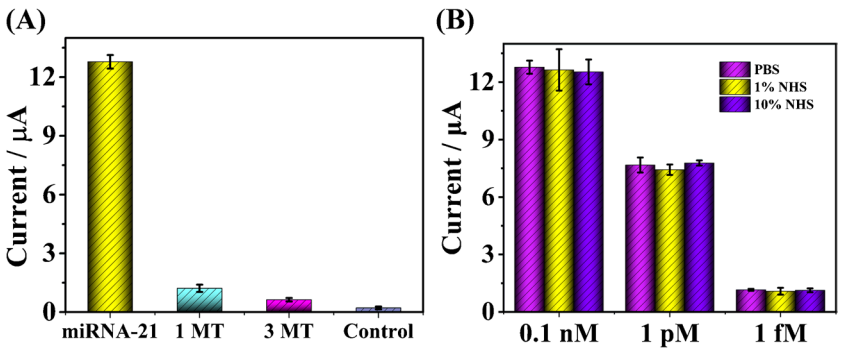

Fig. 5 **A** Analysis of different RNAs (miRNA-21, 1 MT, 3MT) via the proposed electrochemical biosensor. **B** SWV current of Mn-PCN-222-based biosensor at different concentrations of miRNA-21 in 0.1 M PBS, 1% NHS, and 10% NHS. Error bars represent the standard deviations of three repeated measurements

Selectivity and sample for miRNA-21 assay

To test the selectivity of this biosensor, the SWV responses of 0.1 nM miRNA-21, single base mismatch DNA (1 MT), three-base mismatch DNA (3 MT), and blank control were performed. From Fig. 5A, it could be calculated that the current values measured for 1 MT and 3 MT were only 9.992% and 4.483% of that of miRNA-21, respectively. These results showed the proposed electrochemical biosensor owned good selectivity and was capable of identifying single-base mismatch sequences. Moreover, the blank control displayed nearly no SWV response, further suggesting the sensor could distinguish miRNA-21 fragments of distinct sequences. As a result, the Mn-PCN-222-catalyzed ATRP electrochemical biosensor was appropriate for detection of single-nucleotide polymorphisms (SNPs). To assess the anti-interference ability of the proposed biosensor in detection of complicated biological samples, different amounts of miRNA-21 were incubated in PBS, 1% (v/v) diluted healthy human serum (NHS), and 10% (v/v) NHS, respectively. The SWV response current recovery of 0.1 nM, 1 pM, and 1fM miRNA-21 in 10% NHS were 102%, 89.1%, and 98.2%, respectively (Fig. 5B), with all RSDs lower than 9.0%, justifying the anti-interference ability and reproducibility (Table 1). The results showed that the miRNA-21 electrochemical biosensor was feasible for detection in actual biological samples.

Table 1 Real-sample analysis of the proposed biosensor for miRNA-21 spiked in diluted human serum

Sample no.	Added	Mean measured	Mean recovery [a] (%)	RSD (%)
1	0.1 nM	0.102 nM	102	5.16
2	1 pM	0.891 pM	89.1	1.70
3	1 fM	0. 982 fM	98.2	8.91

[a]Recovery (%) = 100 × ($C_{\text{mean measured}}/C_{\text{added}}$)

Reproducibility and stability

Moreover, the reproducibility and stability of the electrochemical biosensor were also validated. As shown in Fig. S5, the inter-assay and intra-assay measure outcomes demonstrated the good repeatability of the proposed biosensor. The inter-assay and intra-assay coefficients of variation were 2.18% and 3.82%, respectively, demonstrating the reliable reproducibility of the biosensor ($n = 3$). As can be seen from Fig. S6, the current density values of the five different electrodes were essentially the same, further demonstrating good repeatability of the proposed sensor. Also, the stability of electrochemical biosensors was investigated. The electrodes were stored at 4°C for 5 days, and the SWV response recovery rate was up to 90.06% with good stability.

Conclusions

In conclusion, a multi-site initiation ATRP method catalyzed by Mn-PCN-222 for miRNA-21 analysis was proposed. Mn-PCN-222 exhibited good catalytic performance due to the ordered combination of metalloporphyrin units and porous structures. Sensitive detection with a broad linear range was acquired via the proposed biosensor. Meanwhile, this biosensor is also efficient in detecting both individual miRNA-21 as well as serum samples. An optimal combination of selectivity, long-term stability, reproducibility, and practicality of the biosensor was discovered. Moreover, detection of other tumor biomarkers could be achieved via simply changing the corresponding DNA sequences, thus supplying a universal electrochemical platform for various biomarkers. In essence, Mn-PCN-222 not only have an easy and efficient synthesis method but also have potential in designing multifunctional electrochemical sensors in the future after combining with host-guest reactions.

Supplementary Information The online version contains supplementary material available at https://doi.org/10.1007/s00604-023-05896-8.

Funding This work was supported by the National Natural Science Foundation of China (Grant Nos. 21974068, 21890740, 21890742, and 9195401).

Data Availability The data available within the article or its supplementary materials.

Declarations

Conflict of interest The authors declare no competing interests.

References

1. Wang M, Herbst RS, Boshoff C (2021) Toward personalized treatment approaches for non-small-cell lung cancer. Nat Med 27(8):1345–1356
2. Organization WH (3 February 2022) Cancer fact sheet. https://www.who.int/news-room/fact-sheets/detail/cancer. Accessed 3 Feb 2022
3. Passaro A, Jänne PA, Mok T, Peters S (2021) Overcoming therapy resistance in Egfr-mutant lung cancer. Nature Cancer 2(4):377–391
4. Falagario UG, Busetto GM, Netti GS, Sanguedolce F, Selvaggio O, Infante B, Ranieri E, Stallone G, Carrieri G, Cormio L (2021) Prospective validation of pentraxin-3 as a novel serum biomarker to predict the risk of prostate cancer in patients Scheduled for prostate biopsy. Cancers 13(7):1611
5. Wang W, Han R, Chen M, Luo X (2021) Antifouling peptide hydrogel based electrochemical biosensors for highly sensitive detection of cancer biomarker Her2 in human serum. Anal Chem 93(19):7355–7361
6. Cheng Z, Choi N, Wang R, Lee S, Moon KC, Yoon S-Y, Chen L, Choo J (2017) Simultaneous detection of dual prostate specific antigens using surface-enhanced Raman scattering-based immunoassay for accurate diagnosis of prostate cancer. ACS Nano 11(5):4926–4933
7. Yang Z, Yu L, Wang Z (2016) Pca3 and Tmprss2-Erg gene fusions as diagnostic biomarkers for prostate cancer. Chin J Cancer Res 28(1):65–71
8. Vykoukal J, Fahrmann JF, Patel N, Shimizu M, Ostrin EJ, Dennison JB, Ivan C, Goodman GE, Thornquist MD, Barnett MJ, Feng Z, Calin GA, Hanash SM (2022) Contributions of circulating micrornas for early detection of lung cancer. Cancers 14(17):4221
9. Meng F, Yu W, Chen C, Guo S, Tian X, Miao Y, Ma L, Zhang X, Yu Y, Huang L, Qian K, Wang J (2022) A versatile electrochemical biosensor for the detection of circulating microrna toward non-small cell lung cancer diagnosis. Small 18(22):e2200784
10. Mahmudunnabi RG, Umer M, Seo K-D, Park D-S, Chung JH, Shiddiky MJA, Shim Y-B (2022) Exosomal microrna array sensor with a bioconjugate composed of p53 protein and hydrazine for the specific lung cancer detection. Biosens Bioelectron 207:114149
11. Cai B, Xia Z, Wang J, Wu S, Jin X (2022) Reduced graphene oxide-based field effect transistor biosensors for high-sensitivity mirna21 detection. ACS Applied Nano Materials 5(8):12035–12044
12. Liu Q, Fan J, Zhou C, Wang L, Zhao B, Zhang H, Liu B, Tong C (2020) Corrigendum to "quantitative detection of mirna-21 expression in tumor cells and tissues based on molecular beacon". Int J Anal Chem 2020:1515794
13. Lv J, Miao Y, Yan G (2017) Detection of tumor marker mirna21 based on phosphorescent resonance energy transfer of Mn–Zns Qds. RSC Adv 7(65):41063–41069
14. Tijunelyte I, Malbec R, Chami B, Cacheux J, Dez C, Leichle T, Cordelier P, Bancaud A (2021) Micro-Rna 21 detection with a limit of 2 Pm in 1 Min using a size-accordable concentration module operated by electrohydrodynamic actuation. Biosens Bioelectron 178:112992
15. Ferdows BE, Patel DN, Chen W, Huang X, Kong N, Tao W (2022) Rna cancer nanomedicine: nanotechnology-mediated Rna therapy. Nanoscale 14(12):4448–4455
16. Li R, Wang H, Liang Q, Chen L, Ren J (2022) Radiotherapy for glioblastoma: clinical issues and nanotechnology strategies. Biomater Sci 10(4):892–908
17. Wang Z, Yan Y, Li C, Yu Y, Cheng S, Chen S, Zhu X, Sun L, Tao W, Liu J, Wang F (2022) Fluidity-guided assembly of Au@Pt on liposomes as a catalase-powered nanomotor for effective cell uptake in cancer cells and plant leaves. ACS Nano 16(6):9019–9030
18. Ambaye AD, Kefeni KK, Mishra SB, Nxumalo EN, Ntsendwana B (2021) Recent developments in nanotechnology-based printing electrode systems for electrochemical sensors. Talanta 225:121951
19. Yan K, Hu Y, Suo Y, Qin Y, Chen X (2022) Magnetoresistance of Ni/Wse2/Ni junctions: robustness against the thickness of Wse2. Nanotechnology 33(38):385001
20. Zhou Z, Mukherjee S, Hou S, Li W, Elsner M, Fischer RA (2021) Porphyrinic Mof film for multifaceted electrochemical sensing. AngewChem Int Ed 60(37):20551–20557
21. Chen Y, Huang W, Wang C, Zhai X, Zhang T, Wang Y, Hu X (2020) Direct growth of poly-glutamic acid film on peroxidase mimicking Pcn-222(Mn) for constructing a novel sensitive non-enzymatic electrochemical hydrogen peroxide biosensor. ACS Sustainable Chem Eng 8(35):13226–13235
22. Demir DF, Monaco A, Foulkes R, Becer CR, Forgan RS (2022) Glycopolymer-functionalized MOF-808 nanoparticles as a cancer-targeted dual drug delivery system for carboplatin and floxuridine. ACS Appl Nano Mater 5(10):13862–13873

23. Mohan B, Kumar S, Xi H, Ma S, Tao Z, Xing T, You H, Zhang Y, Ren P (2022) Fabricated metal-organic frameworks (Mofs) as luminescent and electrochemical biosensors for cancer biomarkers detection. Biosens Bioelectron 197:113738
24. Cai M, Liang W, Wang K, Yin D, Fu T, Zhu R, Qu C, Dong X, Ni J, Yin X (2022) Aperture modulation of isoreticular metal organic frameworks for targeted antitumor drug delivery. ACS Appl Mater Interfaces 14(32):36366–36378
25. Jiang X, He S, Han G, Long J, Li S, Lau CH, Zhang S, Shao L (2021) Aqueous one-step modulation for synthesizing monodispersed Zif-8 nanocrystals for mixed-matrix membrane. ACS Appl Mater Interfaces 13(9):11296–11305
26. Zhang B, Li X, Chen J, Liu T, Cruz A, Pei Y, Chen M, Wu X, Huang W (2021) Tandem synthesis of ϵ-caprolactam from cyclohexanone by an acidified metal-organic framework. ChemCatChem 13(13):3084–3089
27. Iacomi P, Gulcay-Ozcan E, Pires Conti P, Biswas S, Steunou N, Maurin G, Rioland G, Devautour-Vinot S (2022) Mil-101(Cr) Mof as an effective siloxane sensor. ACS Appl Mater Interfaces 14(15):17531–17538
28. Cao Q, Xiao Y, Liu N, Huang R, Ye C, Huang C, Liu H, Han G, Wu L (2021) Synthesis of yolk/shell heterostructures MOF@MOF as biomimetic sensing platform for catechol detection. Sens Actuators B: Chem 329:129133
29. Zhang X, Sun Y, Liu Y, Zhai Z, Guo S, Peng L, Qin Y, Li C (2021) Uio-66-Nh2 Fabrics: Role of Trifluoroacetic Acid as a Modulator on Mof uniform coating on electrospun nanofibers and efficient decontamination of chemical warfare agent simulants. ACS Appl Mater Interfaces 13(33):39976–39984
30. Ma A, Ran H, Wang J, Ding R, Lu C, Liu L, Luo Y, Chen H, Yin T (2022) An urchin-shaped copper-based metalloporphyrin nanosystem as a sonosensitizer for sonodynamic therapy. Nanomaterials 12(2):209
31. Wang L, Qu X, Zhao Y, Weng Y, Waterhouse GIN, Yan H, Guan S, Zhou S (2019) Exploiting single atom iron centers in a porphyrin-like Mof for efficient cancer phototherapy. ACS Appl Mater Interfaces 11(38):35228–35237
32. Hu W-C, Pang J, Biswas S, Wang K, Wang C, Xia X-H (2021) Ultrasensitive detection of bacteria using a 2d MOF nanozyme-amplified electrochemical detector. Anal Chem 93(24):8544–8552
33. Zhang H-W, Zhu Q-Q, Yuan R, He H (2021) Crystal engineering of MOF@COF core-shell composites for ultra-sensitively electrochemical detection. Sens Actuators B: Chem 329:129144
34. Sun H, Qiu Y, Lu Y, Kong J, Zhang X (2020) Ultrasensitive DNA electrochemical biosensor based on Mntbap biomimetic catalyzed Aget Atrp signal amplification reaction. Chem Commun 56(49):6636–6639
35. Min K, Gao H, Matyjaszewski K (2005) Preparation of homopolymers and block copolymers in miniemulsion by Atrp using activators generated by electron transfer (Aget). J Am Chem Soc 127(11):3825–3830
36. Kaupbayeva B, Murata H, Rule GS, Matyjaszewski K, Russell AJ (2022) Rational control of protein–protein interactions with protein-Atrp-generated protease-sensitive polymer cages. Biomacromolecules 23(9):3831–3846
37. Sun H, Qian L, Kong J, Zhang X (2021) Ultra-sensitive nucleic acid detection based on target cycling of triple helix molecular switch and Atrp double signal amplification. Sens Actuators B Chem 337:129791
38. Hu Q, Wang Q, Sun G, Kong J, Zhang X (2017) Electrochemically mediated surface-initiated de novo growth of polymers for amplified electrochemical detection of DNA. Anal Chem 89(17):9253–9259
39. Truong NP, Jones GR, Bradford KGE, Konkolewicz D, Anastasaki A (2021) A comparison of Raft and Atrp methods for controlled radical polymerization. Nat Rev Chem 5(12):859–869
40. Konkolewicz D, Wang Y, Zhong M, Krys P, Isse AA, Gennaro A, Matyjaszewski K (2013) Reversible-deactivation radical polymerization in the presence of metallic copper. A critical assessment of the Sara Atrp and Set-Lrp mechanisms. Macromolecules 46(22):8749–8772
41. Luo J, Durante C, Gennaro A, Isse AA (2021) Electrochemical study of the effect of Al3+ on the stability and performance of Cu-based Atrp catalysts in organic media. Electrochim Acta 388:138589
42. Wang Y-M, Kálosi A, Halahovets Y, Romanenko I, Slabý J, Homola J, Svoboda J, de los Santos Pereira A, Pop-Georgievski O (2022) Grafting density and antifouling properties of poly[N-(2-hydroxypropyl) methacrylamide] brushes Prepared by "grafting to" and "grafting from". Polym Chem 13(25):3815–3826
43. Wang J, Qiu Y, Li L, Qi X, An B, Ma K, Kong J, Zhang X (2022) A Multi−site initiation reversible Addition−fragmentation Chain−transfer Electrochemical Cocaine Sensing. Microchem J 181:107714
44. Boekhoven J, Rubert Perez CM, Sur S, Worthy A, Stupp SI (2013) Dynamic Display of Bioactivity through Host-Guest chemistry. Angew Chem Int Ed 52(46):12077–12080
45. Shang K, Wang X, Sun B, Cheng Z, Ai S (2013) Beta-cyclodextrin-ferrocene host-guest complex multifunctional labeling triple amplification strategy for electrochemical immunoassay of subgroup J of Avian Leukosis Viruses. Biosens Bioelectron 45:40–45